SMALL-ANGLE SCATTERING FROM DETERMINISTIC MASS AND SURFACE FRACTAL SYSTEMS

Eugen M. ANITAS [1, 2] , Azat M. SLYAMOV [1, 3]

[1]Joint Institute for Nuclear Research, Dubna, Moscow Region, Russian Federation
[2] "Horia Hulubei" National Institute of Physics and Nuclear Engineering, Bucharest-Magurele, Romania
[3] Institute of Nuclear Physics, Almaty, Kazakhstan
Corresponding author: Eugen M. ANITAS, E-mail: `anitas@jinr.ru`

Abstract. Structural properties of deterministic mass and surface fractals are studied using small-angle scattering (SAS; X-rays, neutrons) method. The corresponding scattering curves are analyzed in momentum space. The scattering amplitude form a surface fractal can be written as a sum of amplitudes of composing mass fractals. We show that when the distances between scattering units are much larger than their overall dimension, the scattering from a surface fractal can be explained, in a good approximation, in terms of a power-law distribution of the scattering units. We illustrate the above findings on randomly oriented and non-interacting 2D mass and surface fractal systems whose scattering units are equilateral triangles. In our model, the scattering units of the mass fractal are triangles of equal sizes composing the well-known Koch snowflake. For the surface fractal, a sum of triangles of different sizes is considered to form the Koch snowflake.

Key words: small-angle scattering (X-rays, neutrons, light), form factor, mass fractals, surface fractals, Koch snowflake.

1. INTRODUCTION

Various natural nano- and microstructures, such as polymers, colloids, or gels appear similar under a change of scale. The theoretical framework able to describe the scaling behavior of such systems is provided by fractal geometry [1, 2]. Often, the optical, mechanical, statistical or dynamical properties [3–6] are correlated with spatial configurations of the "basic" units (e. g. molecules of *bis*terpyridine [7]) forming the fractal structures. Thus, understanding their microstructural properties has important applications in preparation of nanomaterials with pre-defined functions.

The mathematical modeling of fractal microstructures involves either random (statistical self-similar) or deterministic (exact self-similar) fractals. The most common approach to describe natural structures is to use models of random fractals, such as those generated by ballistic deposition or Eden growth model [8]. However, in the last decade with the advent of nanotechnology, new methods for preparation of nano- and microfractals such as Sierpinski gaskets, Cantor sets, Menger sponge or octahedral structures, have been developed [7, 9–11]. These technological achievements have determined a growing interest in the implementation of existing, and development of new deterministic fractal models, since in this case, they provide a framework that gives "exactly solvable models". In addition, sometimes deterministic models are good approximations for natural processes, such as modeling the transfer across random fractal surfaces [12].

Experimentally, small-angle scattering (SAS; X-rays, neutrons, light) [13, 14] is the preferred method for probing the structure at nano and micro scales for disordered systems, and in particular for fractal systems [15–17]. When X-rays are used, the scattering is mostly determined by the interaction of the incident radiation with electrons. However, in the case of neutrons, the scattering is determined by their interaction with the atomic nuclei and with the magnetic moments in magnetic materials. Basically, SAS yields the elastic cross section per unit solid angle as a function of the magnitude of the scattering vector q, and describes, through a Fourier transform, the spatial density distribution of the investigated sample. When the cross section is normalized to the unit volume of the sample, the scattering intensity $I(q)$ is obtained. Here, $q \equiv (4\pi / \lambda)\sin 2\theta$, λ is the wavelength of the incident radiation, and 2θ is the scattering angle.

Although the loss of information in a scattering experiment is a severe limitation, the SAS method has few important advantages as compared to other structural methods. First, it is a non-invasive method, and usually the investigated samples don't require any special preparation. Second, the physical quantities of interest such as specific surface, radius of gyration or the fractal dimension are averaged over a macroscopic volume. Third, when neutrons are used, SAS has important applications in the study of magnetic properties of materials [18–20]. By exploiting the variation of the neutron scattering lengths, the contrast variation method [21, 22] can be used in biological samples to emphasize or to conceal certain features [23, 24].

In the case of fractal structures, SAS can also distinguish between mass [25] and surface fractals [26]. These two types of structures are revealed through the value of the scattering exponent τ in the fractal region, i. e. in the region in the reciprocal space where the scattering intensity has a simple power-law decay, such as

$$I(q) \propto q^{-\tau}. \tag{1}$$

This holds also for generalized (a superposition of the maxima and minima on a power-law decay) or a succession of generalized power-law decays [27–31]. In a two-phase system in which one phase has a mass fractal dimension D_m and the second phase has the pore fractal dimension D_p, the boundary between phases forms a set of surface dimension D_s. For a mass fractal $D_s = D_m < d$ and $D_p = d$, while in the case of surface fractals $D_m = D_p = d$ and $d - 1 < D_s < d$. Here, d is the Euclidean dimension of the space in which the fractal is embedded. The scattering exponent in Eq. (1) can be written, in terms of the fractal dimensions, as [15, 16]

$$\tau = \begin{cases} D_m, & \text{for mass fractals} \\ 2d - D_s, & \text{for surface fractals} \end{cases} \tag{2}$$

In practice, if the measured scattering exponent from SAS experimental data is $\tau < d$, then the sample has a mass fractal structure, and if the measured exponent is $d - 1 < \tau < d$, then the sample is a surface fractal.

In this work, we calculate the monodisperse SAS intensity from a regular and from a generalized 2D Koch snowflake (KS) surface fractal consisting of mass fractals at various iterations. For regular KS, the distance between its composing structural units (equilateral triangles) are of the same order as their size. For the newly introduced generalized KS, the distances between its composing triangles are much higher than their sizes. By using these models, we show that modeling the surface fractal using a power-law distribution of triangles holds in a good approximation for the generalized KS. The results can be applied to arbitrary surface fractals and with arbitrarily shapes of scattering units that follow a power-law distribution. We explain also how the main structural parameters of surface fractals can be obtained from the scattering intensity.

2. THEORETICAL BACKGROUND

We consider scattering from a system of 2D monodisperse, randomly oriented and non-interacting fractals of scattering length density (SLD) ρ_f and concentration c embedded in a solid matrix of SLD ρ_0. We denote the quantity $\Delta\rho \equiv \rho_f - \rho_0$ the scattering contrast and consider that the total volume irradiated by the incident beam is V'. Then, the elastic cross section per unit volume of the sample (scattering intensity) is given by [13]

$$I(q) \equiv \frac{1}{V'} \frac{d\sigma}{d\Omega} = c \,|\Delta\rho|^2 \, V^2 \left\langle |F(\mathbf{q})|^2 \right\rangle, \tag{3}$$

where $F(\mathbf{q}) \equiv (1/V) \int_V e^{-i\,\mathbf{q}\cdot\mathbf{r}} d\mathbf{r}$ is the normalized scattering amplitude (also known as the normalized form factor) and satisfies the condition $F(0) = 1$ and V is the volume of each fractal. The symbol $\langle \cdots \rangle$ denotes the mean value of the ensemble averaging over all orientations. In spherical coordinates, for 3D orientations and for an arbitrarily function f, the mean value is calculated according to [29]

$$\left\langle f\left(q_x, q_y, q_z\right)\right\rangle = \frac{1}{4\pi}\int_0^\pi \mathrm{d}\theta \sin\theta \int_0^{2\pi}\mathrm{d}\phi f\left(q,\theta,\phi\right), \tag{4}$$

where $q_x = q\cos\phi\sin\theta$, $q_y = q\sin\phi\sin\theta$, and $q_z = q\cos\theta$.

The main properties of mass and surface fractals can be easily understood in terms of generic expressions of the corresponding normalized form factors. In the general case of a mass fractal of fractal dimension D_m and size L, consisting of p scattering units of size l separated by distances d, the SAS intensity can be written as

$$\left\langle \left|F^{(m)}(\mathbf{q})\right|^2\right\rangle \simeq \begin{cases} 1, & q < 2\pi/L \\ (qL/2\pi)^{-D_m}, & 2\pi/L < q < 2\pi/d \\ 1/p, & 2\pi/d < q < 2\pi/l \\ (1/p)(qL/2\pi)^{-4}, & 2\pi/l < q \end{cases} \tag{5}$$

where p is of the order of $(L/d)^{D_m}$. In the case of surface fractals composed of scattering units of maximum size r_0 and minimum size l, the generic expression for the normalized SAS intensity is

$$\left\langle \left|F^{(s)}(\mathbf{q})\right|^2\right\rangle \simeq \begin{cases} 1, & q < 2\pi/r_0 \\ (qr_0/2\pi)^{D_s-6}, & 2\pi/r_0 < q < 2\pi/l \\ (r_0/l)^{D_s-6}(qL/2\pi)^{-4}, & 2\pi/l < q \end{cases} \tag{6}$$

Equations (5) and (6) show that the main feature is the presence of the three main structural regions: the Guinier region at $q < 2\pi/L$ for mass fractals and at $q < 2\pi/r_0$ for surface fractals, the fractal region at $2\pi/L < q < 2\pi/l$ for mass fractals and at $2\pi/r_0 < q < 2\pi/l$ for surface fractals, and the Porod region at $2\pi/l < q$ for both mass and surface fractals. The end of the Guinier region gives information about the overall size of the fractal, the exponent in the fractal region is connected with the fractal dimension (see Introduction section), and the Porod region provides information about the specific surface of the fractal [13]. For the purposes of this paper, our analysis will focus in the interpretation of the scattering intensity in the fractal region.

For a mass-fractal, the normalized scattering amplitude can be written as the product [29]

$$F_n^{(m)}(\mathbf{q}) = F_0(\beta_s^m q r_0)G_1(\mathbf{q})G_1(\beta_s\mathbf{q})\cdots G_1^{n-1}(\beta_s^{n-1}\mathbf{q}), \tag{7}$$

where $F_0(q)$ is the form factor of the scattering unit and $G_1(\mathbf{q})$ is the generative function. The latter one gives the positions of the scattering objects inside the fractal.

Thus, using Eq. (2), the total SAS intensity from a surface fractal can be written as [32, 33]

$$I_m^{(s)}(q) = I_m^{(s)}(0)\left\langle \left|F_m^{(s)}(\mathbf{q})\right|^2\right\rangle, \tag{8}$$

where $I_m^{(s)}(0) \equiv c\left|\Delta\rho\right|^2 V_m^2$, the surface fractal normalized amplitude $F_m^{(s)}(\mathbf{q})$ is a weighted sum of the mass fractal amplitudes given by Eq. (7), and V_m is the volume of the surface fractal at the m-*th* iteration.

It has been recently shown that in the case of a surface fractal at any arbitrary iteration *m* and with scaling factor β_s, the approximation of mass-fractal amplitudes (i.e. when we consider correlations only between scattering units composing a given iteration of the mass fractal) can be written as [32]:

$$I_m^{(s)}(q) \simeq \sum_{n=0}^m V_0^2 \beta_s^{2n(d-D_m)}\left\langle \left|F_n^{(m)}(\mathbf{q})\right|^2\right\rangle, \tag{9}$$

where V_0 is the volume of the scattering unit composing the fractal (or equivalently, the volume of mass fractal at zero-*th* iteration). If the spatial correlations between the scattering units are completely neglected, the approximation of incoherent amplitudes of the scattering units is given by [32, 33]:

$$I_m^{(s)}(q) \simeq \sum_{n=0}^{m} \beta_s^{n(2d-D_m)} I_0(\beta_s^n q), \tag{10}$$

where $I_0(q) \equiv V_0^2 \left\langle \left| F_0^2(\mathbf{q}) \right|^2 \right\rangle$. Figures 1 and 2 show the approximation of the mass fractal amplitudes (black) and the approximation of incoherent amplitudes from a surface fractal (blue dotted) for different values of the control parameter d/l. The scattering intensities for composing mass-fractal are shown for each iteration (red).

Figure 2 shows that by setting up the ratio $d/l = 3$, i.e. by increasing the distance between scattering units three times relative to their size, the approximation of incoherent amplitudes is very good. This indicates that, in general, the SAS from a surface fractal can be written in a good approximation as a sum of intensities of scattering units composing the fractal with the condition that the distances between them are much higher than their size. An important factor for such a good agreement at $d/l = 3$ is that Eqs. (9) and (10) are model-independent and the corresponding fractal region is linear on a double logarithmic scale.
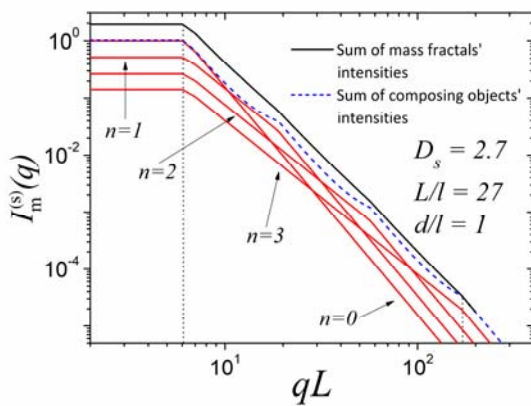

Fig. 1 – Generic SAS from a surface fractal (black), the approximation of incoherent mass-fractals amplitudes (blue dotted), and the intensities of composing mass-fractal iterations (red) for $d/l = 1$.
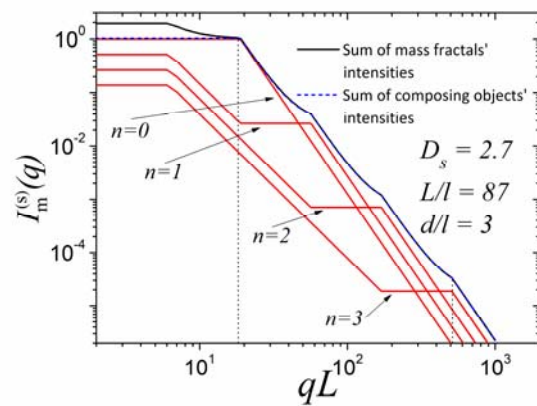
Fig. 2 – Generic SAS from a surface fractal (black), the approximation of incoherent mass-fractals amplitudes (blue dotted), and the intensities of composing mass-fractal iterations (red) for $d/l = 3$.

However, the SAS from KS, or in general from an arbitrarily surface fractal is characterized by a superposition of maxima and minima on a linear power-law decay, in the fractal region. This is also known in the literature as the *generalized power-law decay*. Therefore, a good agreement between the mass-fractal amplitudes and the approximation of incoherent amplitudes for KS can be observed only for $d/l \gg 1$ [33].

3. RESULTS AND DISCUSSIONS

3.1. Construction and properties
of the regular and generalized koch snowflakes

In order to construct the regular two-dimensional KS of overall size L, we adopt here an algorithm which takes into account each mass fractal iteration (Fig. 3, upper part). For this purpose, we start with a single equilateral triangle of edge a and surface area $S = \sqrt{3}a^2/4$. We call this the zero-*th* mass fractal iteration ($n = 0$). First iteration ($n = 1$) is obtained by dividing each edge of the triangle from $n = 0$, into

three segments, each of length $a/3$. Then, an equilateral triangle pointing outward and with base coinciding with the central segment is added to each segment. After the first iteration, the resulting shape is a hexagram, also known as Star of David (black and orange triangles only, in Fig. 3, upper part, $m = 2$). The second iteration ($n = 2$) is obtained by repeating the same procedure to each line segment. In the infinite number of iterations, the fractal dimension is given by

$$D_s = \lim_{m \to \infty} \frac{\log 3 \cdot 4^m}{\log a/a_m} = \frac{\log 4}{\log 3} \simeq 1.26, \tag{11}$$

where $a_m = a/3^m$ is the edge length of the triangle at m-th iteration. Therefore the KS has a finite area given by $S_m = 4S/15(6 - 4^m/9^m)$ which is bounded by an infinite long curve, continuous everywhere but differentiable nowhere. In the limit $m \to \infty$ the area becomes $S^\infty = 2\sqrt{3}a^2/5$ [33].
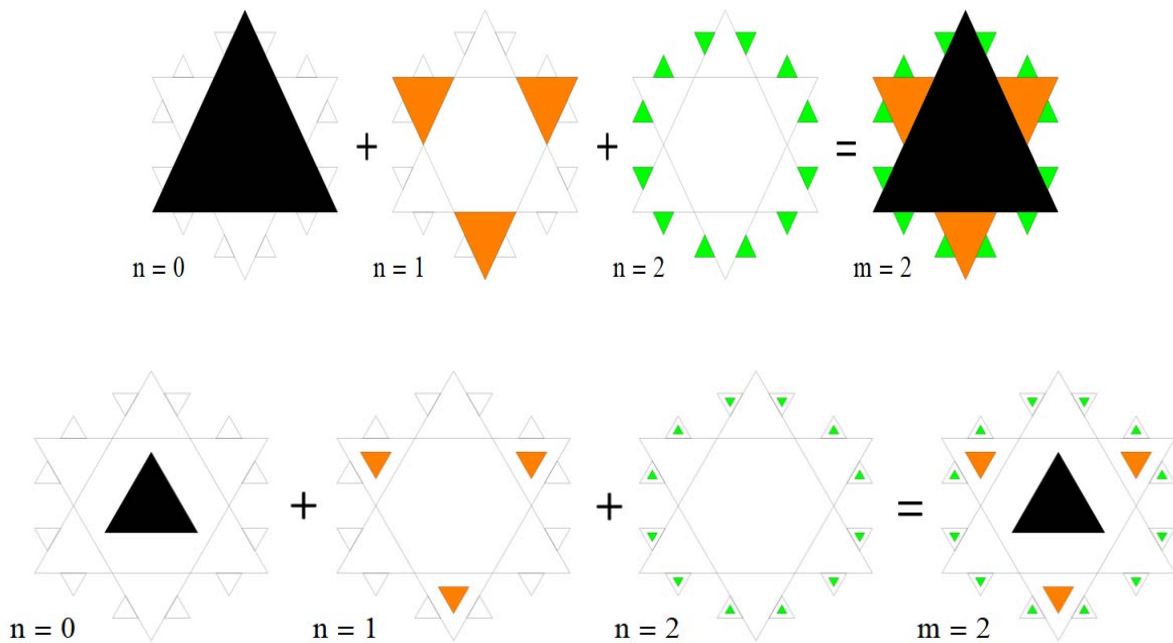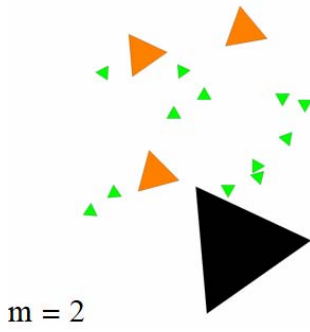

Fig. 3 – Representation of the KS surface fractal at second iteration ($m = 2$)
as a sum of composing mass fractals at iterations $n = 0, 1, 2$. Upper part: regular KS ($L/a \simeq 1$). Lower part:
generalized KS with $L/a > 1$.

Figure 3, upper part, shows the construction of the regular KS surface fractal at ($m = 2$). The figure depicts each composing mass-fractal iteration: $n = 0$ (black), $n = 1$ (orange), and $n = 2$ (green). Note, that in the same figure, the size of the regular KS is approximately the same as of the initial triangle of edge length a, and thus we have $d/l = L/a \simeq 1$. The total scattering intensity (Eq. 8) takes into account the correlations between all the triangles (Fig. 3, upper part, $m = 2$). However, Eq. (9) being the approximation of mass-fractal amplitudes, takes into account only the correlations between the triangles of a given color in Fig. 3, upper part, $m = 2$. Finally, Eq. (10) gives the scattering intensity corresponding to a random distribution of independent triangles, as shown in Figs. 4 and 5. The generalized version of the KS surface fractal is obtained in a similar way, with the exception that the overall size of the KS is much bigger than the size of the initial triangle of edge length a ($n = 0$), and thus $L/a > 1$. As a consequence, the distances between the units composing the KS become much bigger than their sizes. Figure 3, lower part, shows the construction of the generalized KS at ($m = 2$).

Fig. 4 – A random distribution of triangles
forming the 2nd iteration of the KS surface fractal shown in Fig. 3.
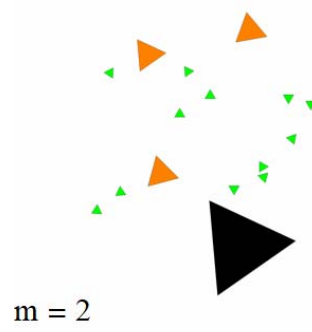
Fig. 5 – The same random distribution as in Fig. 4
but with higher L/a ratio (see text).

3.2. SCATTERING PROPERTIES

For the regular KS, the scattering intensity can be calculated by starting with a recurrence formula for the scattering amplitude $A_m(\mathbf{q}) \equiv S_m F_m^{(s)}(\mathbf{q})$, where S_m is the area of KS at a finite iteration (see above). Thus, provided that the amplitudes at $m = 1$ and $m = 2$ are known, the recurrence formula is given by [33]

$$A_m(\mathbf{q}) = 6G_2(\mathbf{q})\left[\beta_s^2 A_{m-1}(\beta_s \mathbf{q}) - 6G_1(\beta_s \mathbf{q})\beta_s^4 A_{m-2}(\beta_s^2 \mathbf{q}) \right] + \beta_s^2 A_{m-1}(\beta_s \mathbf{q})\left[1 + 6G_1(\mathbf{q}) \right], \qquad (12)$$

where the generative functions are given by $G_1(\mathbf{q}) = (1/6)\sum_{j=0}^5 e^{-i\mathbf{q}\cdot\mathbf{c}_j}$ and $G_2(\mathbf{q}) = (1/6)\sum_{j=0}^5 e^{-i\mathbf{q}\cdot\mathbf{b}_j}$, with $\mathbf{c}_j = (2a/9)\{\cos(\pi(j+1/2)/3), \sin(\pi(j+1/2)/3)\}$ and $\mathbf{b}_j = (2a/3\sqrt{3})\{\cos(\pi j/3), \sin(\pi j/3)\}$. Thus, by inserting Eq. (12) into Eq. (8), the total scattering intensity is obtained (Figs. 6 and 7). We are interested here in the behavior of the scattering curves only in the fractal region.
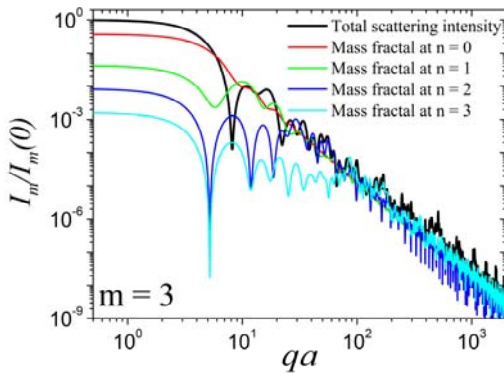
Fig. 6 – SAS from regular KS ($L/a \simeq 1$) at $m = 3$, and intensities
of the four ($n = 0, 1, 2, 3$) mass-fractal iterations.
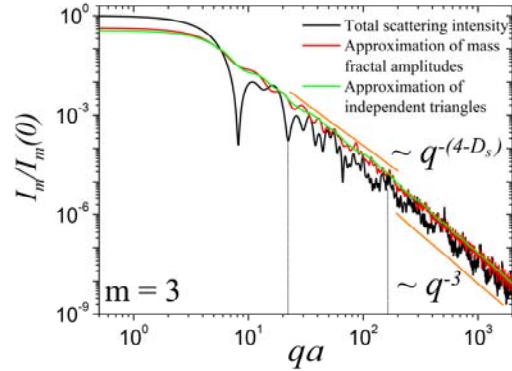
Fig. 7 – SAS from regular KS ($L/a \simeq 1$) at $m = 3$.
Vertical lines show the fractal region.

The results in Figs. 6 and 7 show that the fractal region is at $21 < qa < 180$, and is delimited by vertical lines in Fig. 7. The scattering exponent is $\tau = 2.74$ and it gives the proper value of the surface fractal dimension $D_s = 1.26$, through the relation $\tau = 4 - D_s$ (see Introduction). This value coincides, as expected, with the theoretical value obtained with the help of Eq. (11). Figure 6 shows that the total scattering intensity of KS can be described in terms of contributions from individual mass fractals. A detailed discussion can be found in Ref. [32]. One way to approximate the total intensity is to completely neglect the interference terms in Eq. (8) and to consider the incoherent sum of mass fractal amplitudes (Eq. 9). A rougher approximation is to completely neglect the spatial correlations between composing triangles.

Figure 7 shows that at $L/a \simeq 1$ the approximation of mass fractal amplitudes (Eq. 9) and the approximation of independent units do not give satisfactory approximations (in the fractal region) to the total scattering intensity.

By increasing the ratio L/a, the scattering intensities of each individual mass fractal iteration is characterized by the presence of a second plateau (e.g. at $40 < qa < 100$ in Fig. 8 for $n = 3$). This region arises due to the fact that the distances between individual triangles is much higher than their size and the correlations become less important with increasing q. Similar scattering curves have been observed recently for fat and multiscale fractals [34, 35]. Thus, both the approximations of mass fractal amplitudes and of independent units give a much better agreement with the total scattering intensity (Fig. 9).
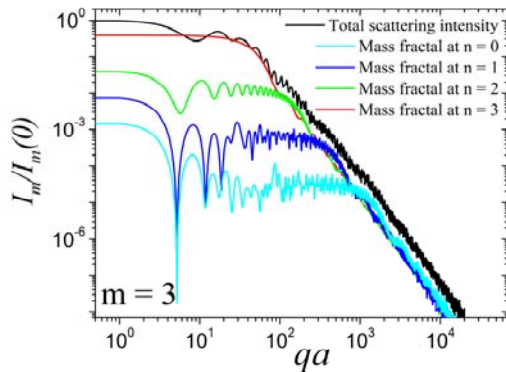

Fig. 8 – SAS from generalized KS ($L/a \simeq 10$) at $m = 3$, and intensities of the four ($n = 0, 1, 2, 3$) mass-fractal iterations.
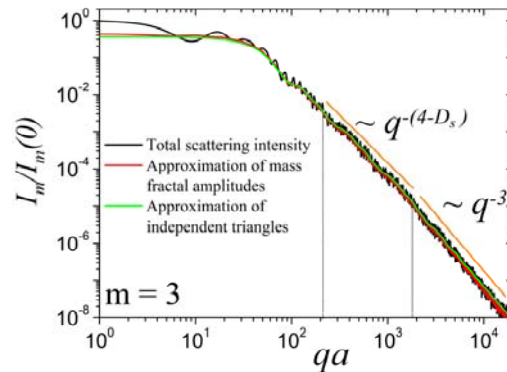
Fig. 9 – SAS from generalized KS ($L/a \simeq 10$) at $m = 3$. Vertical lines show the fractal region.

4. CONCLUSIONS

We introduce a new surface fractal model as a sum of mass fractals, which generalizes the well-known 2D Koch snowflake. Its main feature is that the size of the composing triangles relative to the distances between them can be varied. This is controlled through the ratio L/a, where L is the overall size of the fractal and a is the edge size of the biggest triangle.

We calculate the corresponding SAS intensities and construct two-approximations. For the first one we consider only the incoherent sum of mass fractal amplitudes and for the second one we completely neglect the spatial correlations between composing triangles. We compare the results with scattering from a regular Koch snowflake ($L/a \simeq 1$) and we show that both approximations work very good for the newly introduced model (i. e. when $L/a \gg 1$). This shows that the SAS from a surface fractal can be explained in terms of a power-law type polydispersity of sizes, provided the fine structure of the intensity is neglected.

REFERENCES

1. B. B. MANDELBROT, *The Fractal Geometry of Nature*, W. H. Freeman, New York, 1982.
2. J. FEDER, *Fractals*, Springer, New York, 1988.
3. J. H. LUSCOMBE, R. C. DESAI, *Statistical mechanics of a fractal lattice: Renormalization-group analysis of the Sierpinski gasket,* Phys. Rev. B, **32**, 1614, 1985.
4. C. ALLAIN, M. CLOITRE, *Optical diffraction on fractals*, Phys. Rev. B, **33**, 3566(R), 1986.
5. J. A. SOTELO, V. N. PUSTOVIT, G. M. NIKLASSON, *Optical constants of gold blacks: Fractal network models and experimental data*, Phys. Rev. B, **65**, 245113, 2002.
6. M. GALICEANU, *Relaxation of polymers modeled by generalized Husimi cacti*, J. Phys. A, **43**, 305002, 2010.
7. G. R. NEWKOME, P. WANG, C. N. MOOREFIELD, T. J. CHO, P. MOHAPATRA, S. LI, S. H. HWANG, O. LUKOYANOVA, L. ECHEGOYEN, J. A. PALAGALLO, V. IANCU, S. H. SLA, *Nanoassembly of a Fractal Polymer: A Molecular Sierpinski "Hexagonal Gasket"*, Science, **312**, 1782, 2006.
8. F. FAMILY, T. VICSEK, *Dynamics of Fractal Surfaces*, World Scientific, Singapore, 1991.

9. G. F. CEROFOLINI, D. NARDUCCI, P. AMATO, E. ROMANO, *Fractal Nanotechnology*, Nanoscale Research Letters, **3**, 381, 2008.

10. M. W. TAKEDA, S. KIRIHARA, Y. MIYAMOTO, K. SAKODA, K. HONDA, *Localization of electromagnetic waves in three-dimensional fractal cavities*, Phys. Rev. Lett, **92**, 093902, 2004.

11. E. J. W. BERENSCHOT, H. V. JANSEN, N. R. TAS, *Fabrication of 3D fractal structures using nanoscale anisotropic etching of single crystalline silicon*, J. Micromech. Microeng., **23**, 055024, 2013.

12. M. FILOCHE, B. SAPOVAL, *Transfer across random versus deterministic fractal interfaces*, Phys. Rev. Lett., **84**, 5776, 2000.

13. L. A. FEIGIN, D. I. SVERGUN, *Structure Analysis by Small-Angle X-Ray and Neutron Scattering*, Plenum Press, New York and London, 1987.

14. H. BRUMBERGER, *Modern Aspects of Small-Angle Scattering* (NATO ASI Series, New York, 1995).

15. J. E. MARTIN, A. J. HURD, *Scattering from fractals*, J. Appl. Cryst., **20**, 61, 1987.

16. P. W. SCHMIDT, *Small-angle scattering studies of disordered, porous and fractal systems*, J. Appl. Cryst., **24**, 414, 1991.

17. D. W. SCHAEFER, R. S. JUSTICE, *How Nano Are Nanocomposites?*, Macromolecules, **40**, 8501, 2007.

18. M. L. CRAUS, A. K. ISLAMOV, E. M. ANITAS, N. CORNEI, D. LUCA, *Microstructural, magnetic and transport properties of $La_{0.5}Pr_{0.2}Pb_{0.3-x}SrMnO_2$ manganites*, J. Alloy. Comp., **592**, 121, 2014.

19. Y. TOKUNAGA, X. Z. YU, J. S. WHITE, H. M. RONNOW, D. MORIKAWA, Y. TAGUCHI. Y. TOKURA, *A new class of chiral materials hosting magnetic skyrmions beyond room temperature*, Nature Communications, **6**, 7638, 2015.

20. A. S. CAMERON, Y. V. TYMOSHENKO, P. Y. PORTNICHENKO, J. GAVILANO, V. TSURKAN, V. FELEA, A. LOIDL, S. ZHERLITSYN, J. WOSNITZA, D. S. INOSOV, *Magnetic phase diagram of the helimagnetic spinel compound $ZnCr_2Se_4$ revisited by small-angle neutron scattering*, J. Phys.: Cond. Matt., **28**, 146001, 2016.

21. H. B. STUHRMANN, *Neutron small-angle scattering of biological macromolecules in solution*, J. Appl. Cryst., **7**, 173, 1974.

22. B. JACROT, *The study of biological structures by neutron scattering from solution*, Rep. Prog. Phys., **39**, 911, 1976.

23. A. BOUCHOUX, J. VENTUREIRA, G. GESAN-GUIZOU, F. GARNIER-LAMBROUIN, P. Qu, C. PASQUIER, S. PEZENNEC, R. SCHWEINS, B. CABANE, *Structural heterogeneity of milk casein micelles: a SANS contrast variation study*, Soft Matter, **11**, 389, 2015.

24. E. M. RATH, A. P. DUFF, E. P. GILBERT, G. DOHERTY, R. B. KNOTT, W. B. CHURCH, *Neutron scattering shows a droplet of oleic acid at the center of the BAMLET complex*, Proteins: Structure, Functions, Bioinformatics, **85**, 1371, 2017.

25. J. TEIXEIRA, *Small-angle scattering by fractal systems*, J. Appl. Cryst., **21**, 781, 1988.

26. H. D. BALE, P. W. SCHMIDT, *Small-Angle X-Ray-Scattering Investigation of Submicroscopic Porosity with Fractal Properties*, Phys. Rev. Lett., **53**, 596, 1984.

27. G. BEAUCAGE, *Approximations leading to a Unified Exponential/Power-Law Approach to Small-Angle Scattering*, J. Appl. Cryst., **28**, 717, 1995.

28. G. BEAUCAGE, *Small-Angle Scattering from Polymeric Mass Fractals of Arbitrary Mass-Fractal Dimension*, J. Appl. Cryst., **29**, 134, 1996.

29. A. YU. CHERNY, E. M. ANITAS, V. A. OSIPOV, A. I. KUKLIN, *Deterministic fractals: Extracting additional information from small-angle scattering data*, Phys. Rev. E, **84**, 036203, 2011.

30. E. M. ANITAS, *Small-angle scattering from fat fractals*, Eur. Phys. J. B, **87**, 139, 2014.

31. E. M. ANITAS, *Scattering structure factor from fat fractals*, Rom. J. Phys., **60**, 647, 2015.

32. A. YU. CHERNY, E. M. ANITAS, V. A. OSIPOV, A. I. KUKLIN, *Scattering from surface fractals in terms of composing mass fractals*, J. Appl. Cryst., **50**, 919, 2017.

33. A. YU. CHERNY, E. M. ANITAS, V. A. OSIPOV, A. I. KUKLIN, *Small-angle scattering from the Cantor surface fractal on the plane and the Koch snowflake*, Phys. Chem. Chem. Phys., **19**, 2261, 2017.

34. E. M. ANITAS, A. SLYAMOV, R. TODORAN, Z. SZAKACS, *Small-Angle Scattering from Nanoscale Fat Fractals*, Nanoscale Research Letters, **12**, 389, 2017.

35. E. M. ANITAS, A. SLYAMOV, *Structural characterization of chaos game fractals using small-angle scattering analysis*, PLOS ONE, **12**, e0181385, 2017.